LBL-11629

Lawrence Berkeley Laboratory
UNIVERSITY OF CALIFORNIA

Materials & Molecular Research Division

Presented at the Annual Meeting of The Metallurgical Society/AIME Societies, Chicago, IL, February 22-26, 1981; and to be published in Metallurgical Transactions

HIGH RESOLUTION SCANNING AUGER MICROSCOPIC INVESTIGATION OF INTERGRANULAR FRACTURE IN AS-QUENCHED Fe-12Mn

H.J. Lee and J.W. Morris, Jr.

February 1981

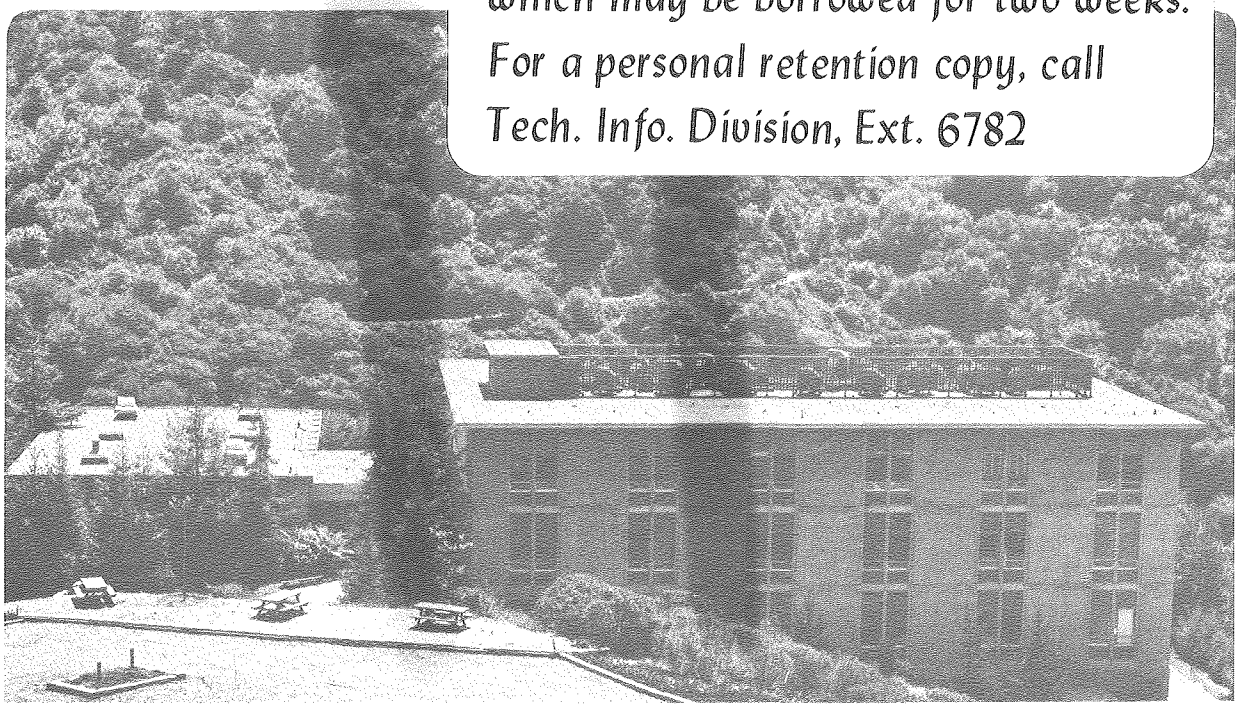

Prepared for the U.S. Department of Energy under Contract W-7405-ENG-48

DISCLAIMER

HIGH RESOLUTION SCANNING AUGER MICROSCOPIC INVESTIGATION OF INTERGRANULAR FRACTURE IN AS-QUENCHED Fe-12Mn

By

H. J. Lee and J. W. Morris, Jr.

Materials & Molecular Research Division
Lawrence Berkeley Laboratory

and

Dept. of Materials Science & Mineral Engineering
University of California, Berkeley

This work was supported by the Director, Office of Energy Research, Office of Basic Energy Science, Material Sciences Division of the U.S. Department of Energy under Contract Number W-7405-ENG-48.

ABSTRACT

Previous research in this laboratory led to the conclusion that the low temperature intergranular fracture mode in Fe-Mn alloys is microstructurally determined, and does not require metalloid segregation or other chemical contamination. That conclusion was tested in the present investigation, which used high resolution scanning Auger microscopy to study the intergranular fracture surfaces. The fracture mode at liquid nitrogen temperature was found to be intergranular fracture whenever the alloy was quenched from the austenite field, irrespective of the austenization time or temperature. High resolution chemical analyses of the intergranular fracture surfaces failed to reveal any consistent segregation of P, S, O, or N. The occasional appearance of sulfur or oxygen on the fracture surface was found to be due to a low density precipitation of MnS and MnO_2 along the prior austenite grain boundaries. Excepting these dispersed precipitates, there was no evidence of manganese enrichment of the prior austenite grain boundaries. A slight segregation of carbon was found along the grain boundaries, but does not appear to be implicated in the tendency toward intergranular fracture. The present results hence reinforce the conclusion that the low temperature intergranular fracture of Fe-12Mn is microstructurally determined.

INTRODUCTION

The low temperature mechanical properties of Fe-Mn alloys have been the subject of active research over the last several years (1-4). This research is motivated by the potential economic benefit from replacing nickel by manganese in cryogenic structural steels and by the possibility that austenitic grades of Fe-Mn may offer particular advantages in structural applications at 4K. The research in this laboratory (5-9) has concentrated on the development of ferritic grades having manganese contents in the range 5-12 wt.%.

One intriguing feature of the Fe-Mn system (5-8) is the anomalous change in its mechanical properties as the manganese content is increased from 8 to 12 wt.%. While the alloy yield strength increases monotonically over this composition range, the ductile-brittle transition temperature falls (Fig. 1). At the same time the fracture mode below the ductile-brittle transition temperature changes from a typical transgranular cleavage at the 8% manganese level to a virtually complete intergranular failure in the 12% manganese alloy (Fig. 2). The Fe-Mn system hence provides the only example known to us in which a simultaneous increase in strength and shift to an intergranular brittle fracture mode is associated with a decrease in the ductile-brittle transition temperature.

The as-quenched microstructure of the Fe-Mn binary also changes dramatically over the 8-12% manganese range. At 8% manganese the alloy quenches into the dislocated lath martensite structure shown in Fig. 3a, while at 12 wt.% manganese the as-quenched structure is the irregular blocky martensite shown in Fig. 3b. The change in microstructure appears to be associated with the intrusion of the hexagonal ε-martensite phase, which first appears

at approximately 10 wt.% manganese, precedes the α' martensite in the transformation sequence, and, along with a slight admixture of residual austenite phase, forms the block boundaries of the blocky martensite structure (Fig. 4) (8).

It is therefore natural to seek an interpretation of the anomalous change in the mechanical properties of the alloy in terms of the striking changes in its microstructure. Such an interpretation was proposed by Hwang and Morris (8) after a careful investigation of the microstructure and intergranular fracture mode in Fe-12Mn. They suggested that the lowering of the ductile-brittle transition temperature as the manganese content is raised from 8 to 12 wt.% is due to an effective grain refinement caused by the shift to the irregular blocky martensite structure. In this interpretation the intergranular failure is not due to any catastrophic weakness of the grain boundaries, but rather to the fact that the toughening of the matrix has the consequence that the intergranular fracture path is the "weak link" in the alloy. Low resolution Auger spectroscopic studies of the intergranular fracture surface failed to reveal any consistent chemical segregation on the grain boundary, and it was therefore concluded that the intergranular fracture path is not only the "weak link" in the structure but is inherently so.

A knowledgeable referee who reviewed reference 8 for Metallurgical Transactions was prepared to accept, provisionally, the microstructural interpretation of the intergranular fracture mode, but felt that a reinvestigation of the intergranular surface using more sensitive Auger spectroscopy than was available to us at that time would nonetheless reveal a metalloid contaminant source for the intergranular failure in the as-quenched condition.

He particularly noted weak metalloid peaks present in some of the Auger spectra presented in ref. 8. The present research was undertaken to clarify this issue through high resolution Auger spectroscopic studies of the intergranular fracture surface in Fe-12Mn.

EXPERIMENTAL PROCEDURE

Alloys of nominal composition Fe-12 wt.% Mn were cast after induction melting in an argon gas atmosphere. The impurity levels in the alloy were maintained at the lowest practical levels to reduce their possible effects, and are given in Table I. After casting, the ingots were homogenized in vacuum at 1200°C for 25 hrs, and then upset cross-forged at 1100°C to 25 mm thickness. Blanks cut from these plates were austenized for 2 hrs at temperatures ranging from 850-1200°C to determine the influence of austenization temperature and were austenitized for times up to 100 hrs at 1100°C to determine the effect of austenization time. The blanks were then water quenched to room temperature.

Following heat treatment specimens of two types were cut from the as-quenched blanks. ASTM standard Charpy V-notch specimens were cut longitudinal to the rolling direction and broken by impact at liquid nitrogen temperature (-196°C). Specimens for Auger analysis were machined from the longitudinal direction 32.0 mm length and 3.68 mm diameter, then notched 3.05 mm for *in situ* fracture in the specimen chamber.

Microstructural and fractographic analyses were conducted using standard optical, transmission electron microscopic, and scanning electron microscopic techniques. An energy-dispersive x-ray spectrometer (EDAX) was used for chemical analysis of precipitates on the fracture surface of broken Charpy specimens.

High resolution chemical analyses of the intergranular fracture surface and depth profiles of the grain boundary composition were made in a PHI model 590 scanning Auger microscope. An in situ fracture stage was used to prepare fresh fracture surfaces in an ultra high vacuum of approximately 6 x 10^{-10} Torr. The analyses were done using a primary electron energy of either 2 kV or 5 kV, and an electron beam whose size was controlled at 0.3 to 2 μm depending on the nature of the region to be analyzed. At least 10 points on each intergranular fracture surface were selected by scanning electron microscopy and analyzed with 0.3% energy resolution. The peak-to-peak modulation used was either 3 eV or 6 eV depending on the energy scanning range. The time constant was 0.003 sec. and the energy sweep rate was 0.5 eV/sec. In most cases, the data was automatically accumulated in the MAC system provided with the model 590 using the parameters: Time/point = 50 msec, peak-to-peak modulation = 6 eV, and volt/step = 1 eV. Chemical composition of the fracture surface was obtained from Auger peak-to-peak amplitude of each element and its relative sensitivity (10). The depth profiles were made by sputtering with purified argon gas using a primary iron energy of 1 or 3 kV and an ion beam size of 200 microns. The residual gas detector of a 3M model 710 SIMS was used to analyze the chemical composition of the residual gas of the ultra high vacuum reaction chamber.

RESULTS AND DISCUSSION

A. The Influence of Austenitizing Conditions on the Fracture Mode.

To determine the influence of austenitizing conditions on the fracture mode at -196°C, samples of Fe-12Mn were austenitized for 2 hrs at temperatures from 850-1200°C, and for 100 hrs at 1100°C, before water quenching to room temperature. The samples were then cut into Charpy impact specimens for fracture at -196°C and into notched specimens for cold in situ fracture in the high vacuum chamber of the scanning Auger microscope. Results of these studies are presented in Figs. 5 and 6. The change in austenization

temperature from 850 to 1200°C changed the prior austenite grain size from approximately 15 μm to approximately 250 μm but did not significantly change the alloy hardness, the Charpy impact value at -196°C, or the brittle-fracture mode, which was essentially complete intergranular failure in all cases. The specimen given extended aging at 1100°C also showed complete intergranular fracture.

B. The Chemical Composition of The Intergranular Fracture Surface.

1. Segregation of common metalloid impurities. Chemical analyses of the intergranular fracture surfaces were made using high resolution scanning Auger microscopy (SAM) as described above. A typical Auger spectrum is shown in Fig. 7 along with a SEM fractograph taken from the SAM. The characteristic Auger electron peaks of the metalloid impurities usually associated with intergranular embrittlement, S, P, As, Sb, and Sn (11-13), are absent from this and other high resolution Auger spectra taken on these fracture surfaces. The only apparent segregant is carbon, which is responsible for the small peak at 272 eV. The common metalloid impurities are also absent from high resolution Auger spectra taken from the intergranular fracture surface of the specimen annealed for 100 hrs at 1100°C (Fig. 8), though in this case a small nitrogen peak is found at 379 eV.

Significant sulfur and oxygen peaks were, however, occasionally found in low resolution Auger spectra made using a relatively large primary beam size (~10 μm). The fact that these peaks are absent from the high resolution spectra suggested that they might be due to sulfide or oxide inclusions in the grain boundary. Two types of small, spherical inclusions were found to be present in low density on the intergranular fractur surface, as shown in Fig. 9. The EDAX analysis included in the figure reveals that one set of

inclusions (type 2) is essentially MnS, while the second (type 1) is a Mn-rich inclusion which may be an oxide or carbide. A more detailed Auger spectroscopic analysis is given in Fig. 10, which shows the comparative spectra of inclusions of each of the two types (labelled 1 and 2), a depression from which an inclusion has apparently been removed (labelled 3), and the matrix away from these defects (labelled 4). The spectra show that precipitate 1 is nearly MnS while precipitate 2 is basically MnO_2, with a small addition of S (possibly a surface component). The hole labelled 3 contains S, O, N, and C, which appear to have co-segregated at the inclusion matrix interface. The grain boundary away from the inclusions (region 4) is essentially free of S, O, and N.

These observations show that the intergranular fracture surface of the as-quenched specimens is essentially free of common metalloid impurities except where sulfide or oxide inclusions are present. These inclusions are present in a relatively low density and show no evidence of deformation or fracture; they do not appear to promote or influence intergranular fracture in any significant way.

2. Segregationof Mn, C, and N. The possible segregation of Mn, C, and N was given particular attention in this work since carbon is found to segregate and since Mn and N co-segregation during tempering has been cited (14) as a dominant cause of temper embrittlement in Fe-Mn steels. To examine the segregation of these species high resolution chemical analyses of the intergranular fracture surfaces were supplemented by Ar^+ sputtering studies to determine the composition profile adjacent to the surface. For these analyses the surfaces were sputtered at a rate of ~100 Å/min (measured on a Ta_2O_5 standards). Results of the sputtering studies are presented

in Figs. 11 and 12, and the resulting composition profiles are shown in Fig. 13.

Analysis of the Mn concentration shows that the Mn content of the fractured grain boundary is nearly equal to that in the bulk, and the Mn composition is nearly constant with depth below the fracture surface (Fig. 13). While there is prior evidence (5,14) for Mn accumulation in the prior austenite grain boundaries when martensitic Fe-Mn alloys are tempered, the present results show no significant grain boundary accumulation of Mn during annealing in the austenite phase, even when that annealing is done for 100 hrs at 1100°C.

Carbon, on the other hand, apparently does segregate to the austenite grain boundaries during annealing in the austenite phase. A carbon peak was consistently found in the high resolution Auger spectra taken from all fracture surfaces examined. The consistency of the carbon peak led to an investigation of its possible source in the contaminant gas of the instrument, particularly via carbon monoxide decomposition on the cold, fresh fracture surface. But while CO is present in the residual vapor (Fig. 14), the vacuum levels used in this work (5×10^{-10} to 1×10^{-9} Torr) the carbon peak was consistent in amplitude and oxygen peaks were absent for ~20 min. after fracture.

The carbon concentration on the intergranular fracture surface was small but independent of austenization temperature or time for the range of conditions studied. The intergranular carbon concentration did vary slightly with the bulk carbon content, from ~0.4 at.% in an alloy with 30 ppm C to ~0.6 at.% in an alloy with 190 ppm C. The sputter profile (Fig. 13) shows that the carbon is confined to the immediate vicinity of the intergranular fracture surface, and reaches its bulk composition

within 30 Å of the surface. Previous researchers (15,16) have suggested that the chemical state of the carbon can be determined from the shape of the Auger peak. The Auger peak shape (Fig. 15) resembles that which these workers associate with carbide rather than free carbon. But given the uniformity of the carbon distribution, its low concentration, and the absence of carbide-forming co-segregants, it seems likely that the Auger peak shape reflects the nature of carbon bonding in the grain boundary rather than showing the presence of any definable carbide.

Nitrogen segregation was found only in the specimens which had been austenitized for very long time (100 hrs at 1100°C) and at inclusion interfaces. The nitrogen profile resembles that of carbon (Fig. 13); where nitrogen is found, it is narrowly confined to the intergranular region.

DISCUSSIONS AND CONCLUSIONS

The results of this investigation generally support the hypothesis advanced in ref. 8: that the preference for an intergranular fracture mode in the brittle fracture of Fe-12Mn is an inherent property of the alloy (microstructurally determined) rather than a consequence of chemical contamination of the grain boundaries. While there is evidence that the segregation of species such as S, P, Mn, and N promotes intergranular fracture, the present results show that such segregation is not necessary; intergranular fracture occurs in the absence of a detectable grain boundary accumulation of any of these species.

The role of carbon, however, remains uncertain. While carbon is generally believed to promote grain boundary cohesion (17) carbide formation can contribute to intergranular embrittlement (18,19). In the present case the carbon concentration on the intergranular fracture surface is small, and if

there is a carbide, it is a subtle one. Nonetheless the carbon accumulation is consistent and may contribute to the strong preference for intergranular fracture. Its role needs further investigation.

ACKNOWLEDGMENTS

This work was supported by the Director, Office of Energy Research, Office of Basic Energy Science, Material Science Division of the U. S. Department of Energy under contract #W7405-ENG-48.

REFERENCES

1. M. J. Schanfein, M. J. Yokota, V. F. Zackay, E. R. Parker, and J. W. Morris, Jr.: Properties of Materials for Liquified Natural Gas Tankage, ASTM STP 579, 1975, p. 361.
2. H. Yoshimora, N. Yamada, and H. Yada: Trans. Iron Steel Inst. Japan, 1976, vol. 15, p. 464.
3. R. L. Tobler, H. J. McHenry, and R. P. Reed: Advances in Cryogenic Engineering, 1978, vol. 24, p. 560.
4. J. W. Morris, Jr., S. K. Hwang, K. A. Yuschenko, V. T. Belotzerkovetz, and O. G. Kvasnerskii: Advances in Cryogenic Engineering, 1978, vol. 24, p. 91.
5. S. K. Hwang: Ph.D. Thesis, Dept. of Materials Science and Engineering, University of California, Berkeley, 1977, LBL Report No. 6603.
6. S. K. Hwang and J. W. Morris, Jr.: Met. Trans., 1979, vol. 10A, p. 545.
7. S. K. Hwang and J. W. Morris, Jr.: Advances in Cryogenic Engineerig, 1978, vol. 24, p. 137.
8. S. K. Hwang and J. W. Morris, Jr.: Met. Trans., 1980, vol. 11A, p. 1197.
9. M. Niikura and J. W. Morris, Jr.: Met. Trans., 1980, vol. 11A, p. 1531.
10. L. E. Davis, N. C. MacDonald, P. W. Palmberg, G. E. Riach, and R. E. Weber, eds. Handbook of Auger Electron Spectroscopy, 2nd ed., 1976, Eden Prairie, Minn., p. 9276.
11. A. Joshi and D. F. Stein: Temper Embrittlement of Alloy Steels, ASTM STP, 1972, vol. 499, p. 59.
12. H. L. Marcus, L. H. Hackett, Jr. and P. W. Palmberg: ibid., p. 90.
13. C. J. McMahon, Jr.: Grain boundaries in Engineering Metals, eds. J. L. Walter, J. H. Westbrook and D. A. Woodford, Claitors Pub. Co., New Orleans, 1975, p. 525.

14. J. D. Bolton, E. R. Petty, and G. B. Allen: Met. Trans., 1971, vol. 2, p. 2915.

15. C. C. Chang: Characterization of Solid Surfaces, Kane & Larrabee, eds. Plenum, 1974, p. 509.

16. D. F. Stein, W. C. Johnson, and C. L. White: Grain boundary structure and properties, G. A. Chadwick and D. A. Smith, eds., New York, Academic Press, 1976, p. 301.

17. C. J. McMahon, Jr.: Acta Met., 1966, vol. 14, p. 839.

18. S. K. Banerji, C. J. McMahon, Jr., and H. C. Feng: Met. Trans., 1978, vol. 9A, p. 237.

19. C. L. Briant and S. K. Banerji: Met. Trans., 1979, vol. 10A, p. 1151.

FIGURE CAPTIONS

1. Change in the ductile-brittle transition temperature as a function of manganese contents in Fe-Mn alloys.
2. Scanning electron fractographs taken from Charpy specimens tested at -196°C (a) Fe-8Mn (b) Fe-12Mn.
3. Transmission electron micrographs showing (a) the dislocated lath martensite structure of quenched Fe-8Mn and (b) the blocky martensite structure of Fe-12Mn.
4. Bright field (a) and dark field (b) transmission electron micrographs showing ε-martensite plates defining blocks of α' martensite in Fe-12Mn
5. Changes of microstructures and properties of Fe-12Mn after austenitizing for 2 hours: (a) prior austenite grain size (b) hardness at room temperature (c) Charpy impact energy at -196°C.
6. Scanning electron fractographs of Charpy specimens tested at -196°C after austenitizing for two hours at (a) 850°C (b) 1000°C (c) 1100°C (d) 1200°C followed by water quenching.
7. Auger electron spectrum obtained from an intergranular fracture surface of an austenitized (1100°C/2 hr/WQ) specimen; the comparison scanning electron fractograph was taken from the SAM.
8. Auger electron spectrum obtained from the intergranular fracture surface of an austenitized (1100°/100 hr/WQ) specimen.
9. SEM-EDAX analysis of particles on the intergranular fracture surface.
10. SEM-AES analysis of four different regions on the intergranular fracture surface.
11. Auger electron spectra obtained from (a) the fresh fracture surface and (b) the sputtered surface of an austenitized (1100°/2 hr/WQ) specimen.

13. Sputtering profiles obtained from the intergranular surface of the specimen austenitized at 1100°C (a) for 2 hours and (b) for 100 hours.
14. Residual gas analysis of the reaction chamber vapor at ultra-high vacuum (6×10^{-10} Torr).
15. Partial auger electron spectrum obtained from the intergranular fracture surface of an austenitized (1100°C/2 hr/WQ) specimen using high sensitivity.

TABLE I.

Impurity Levels

WT.%

C	N	O	P	S
0.003	0.005	0.004	0.007	0.006
0.019	0.001	0.004	0.008	0.006

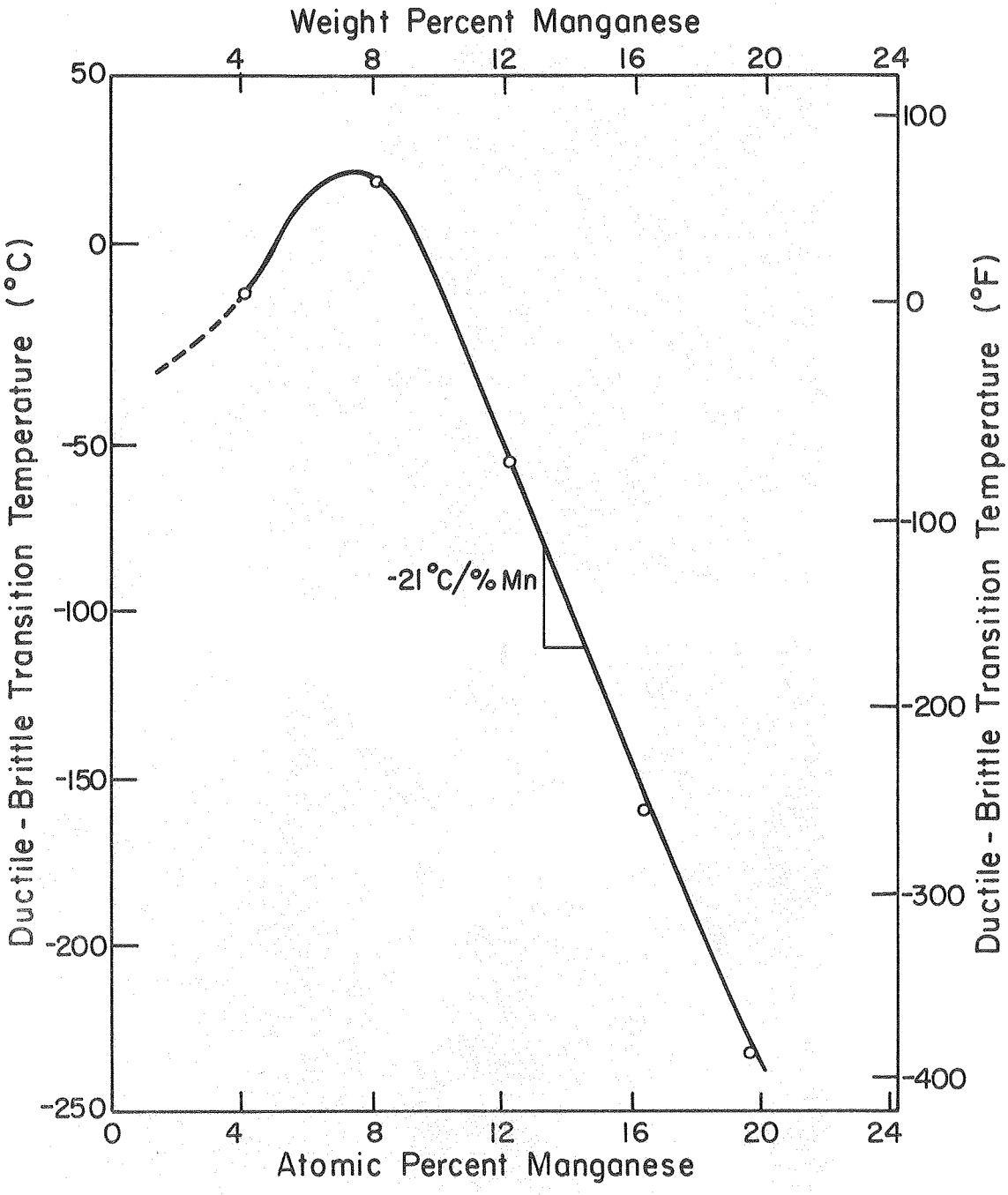

Figure 1

XBL 747-6667

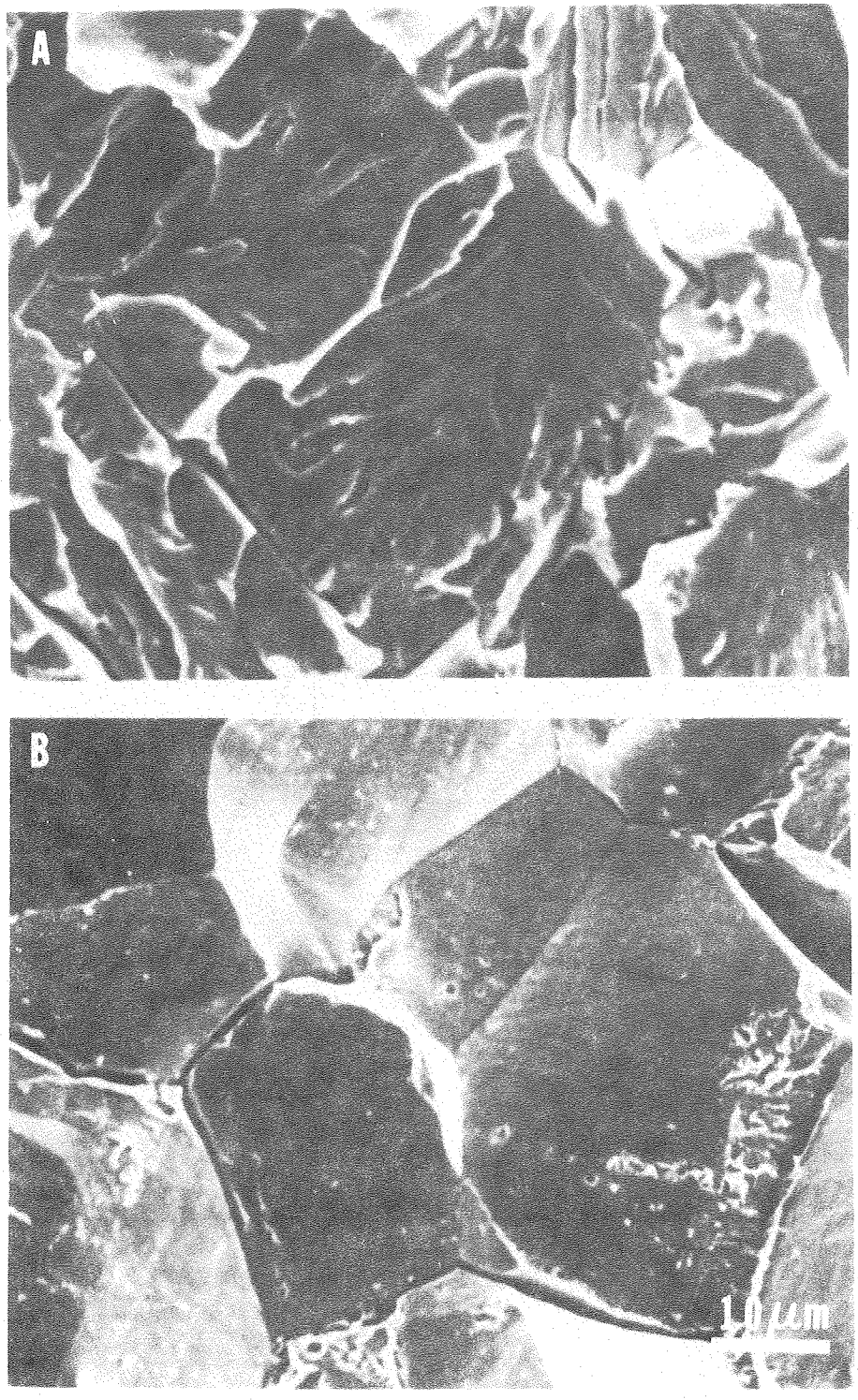

XBB 810-11418

Figure 2

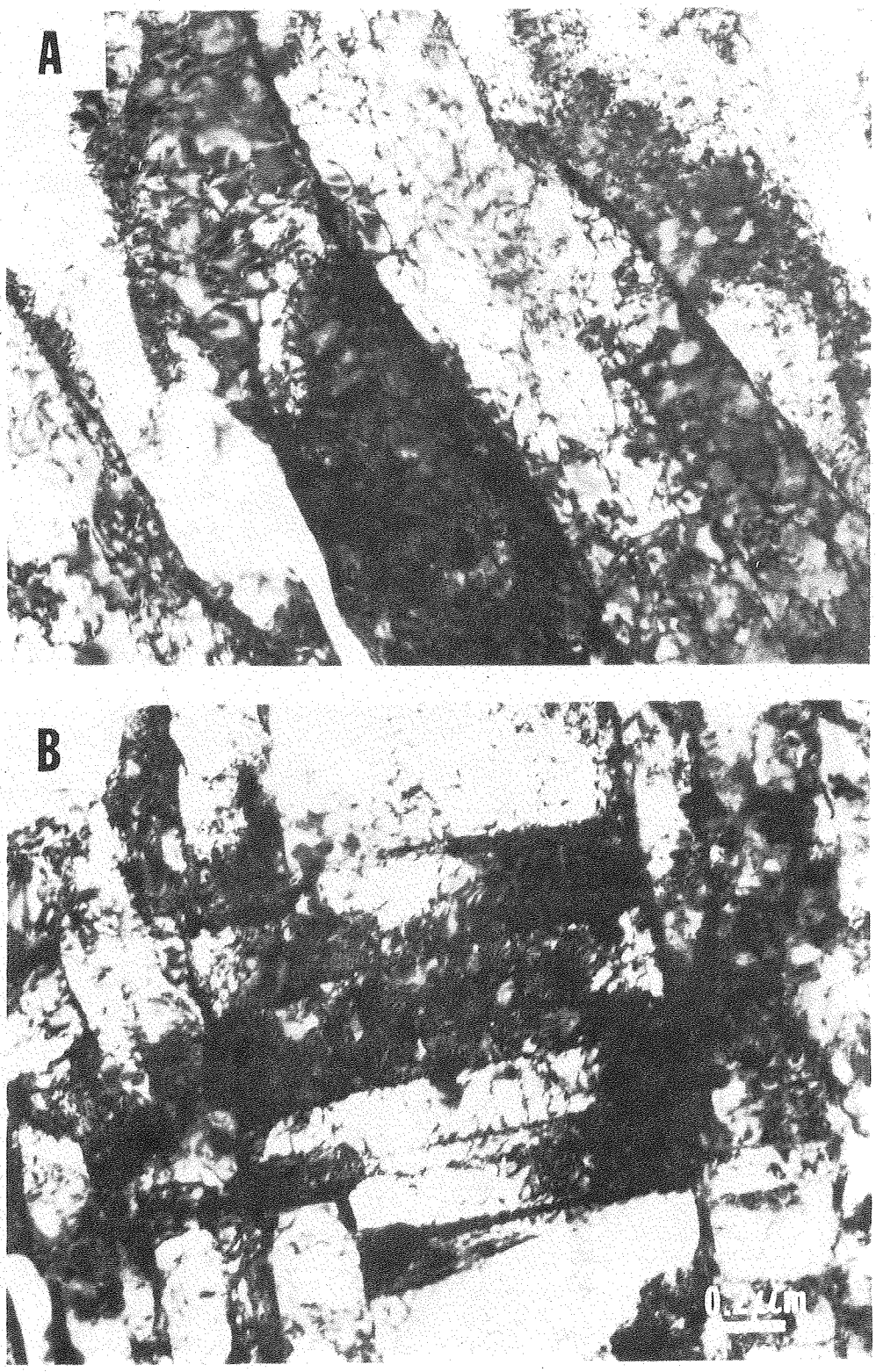

XBB 810-11420

Figure 3

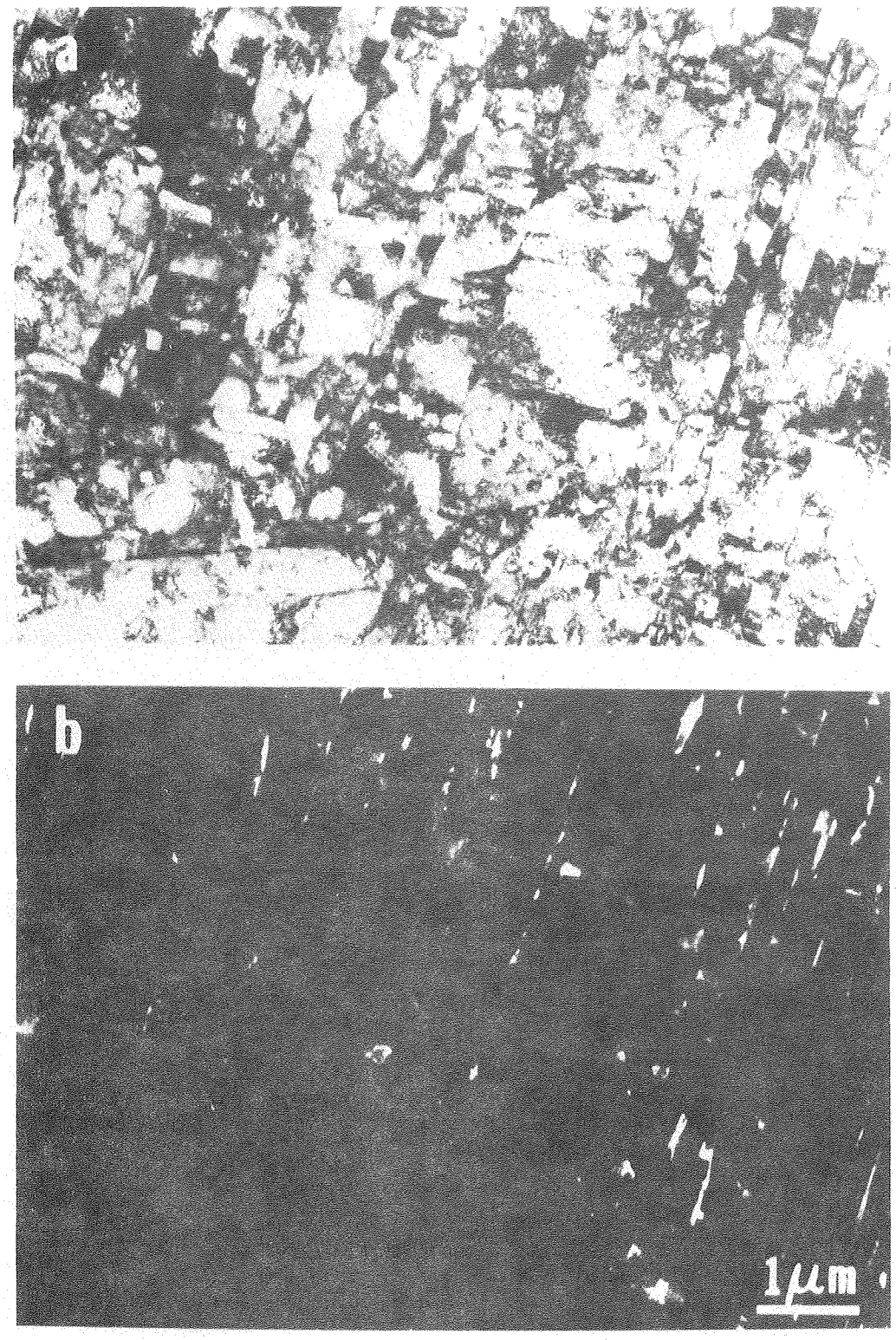

XBB 810-11419

Figure 4

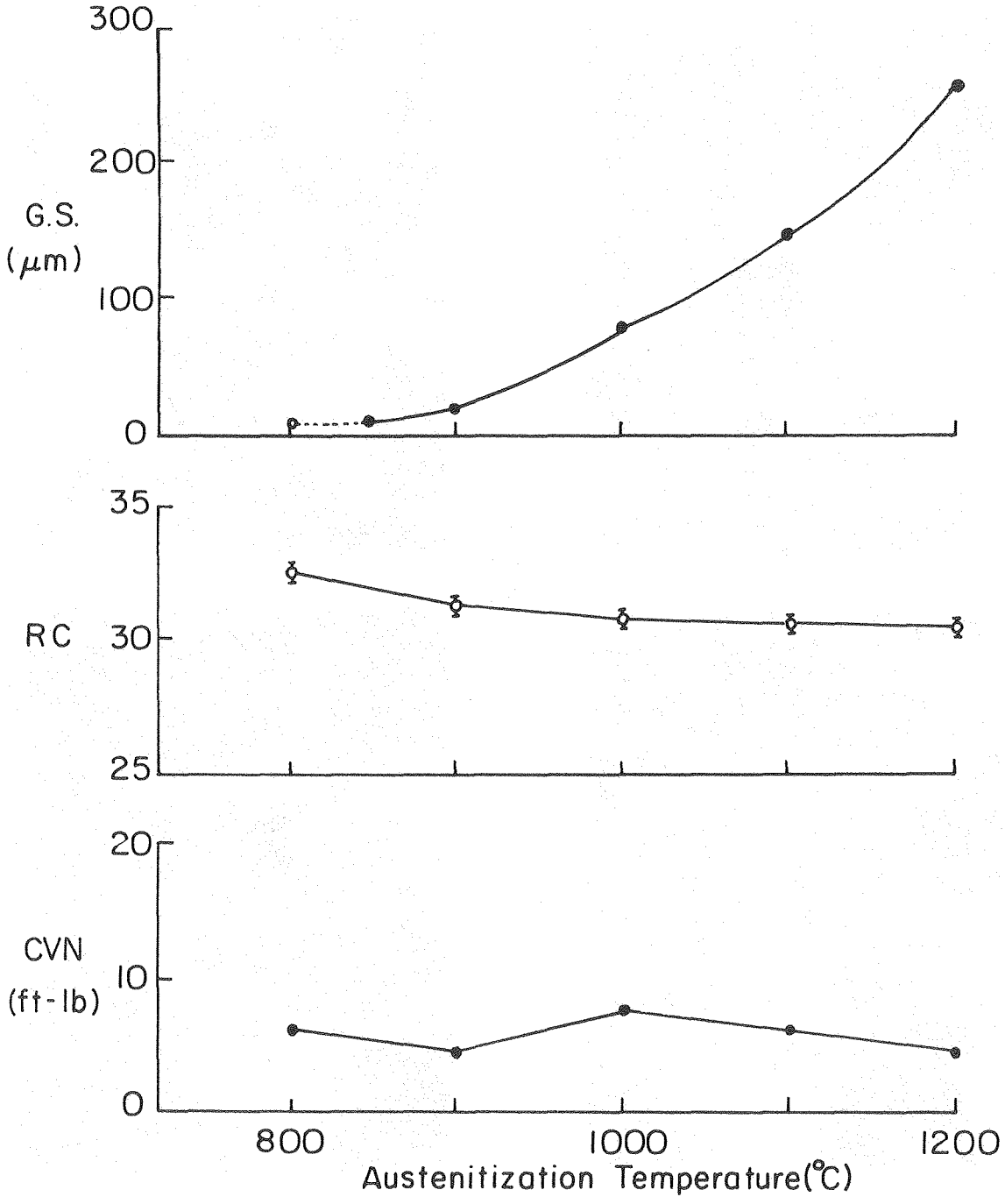

Figure 5

XBL 8010-6241

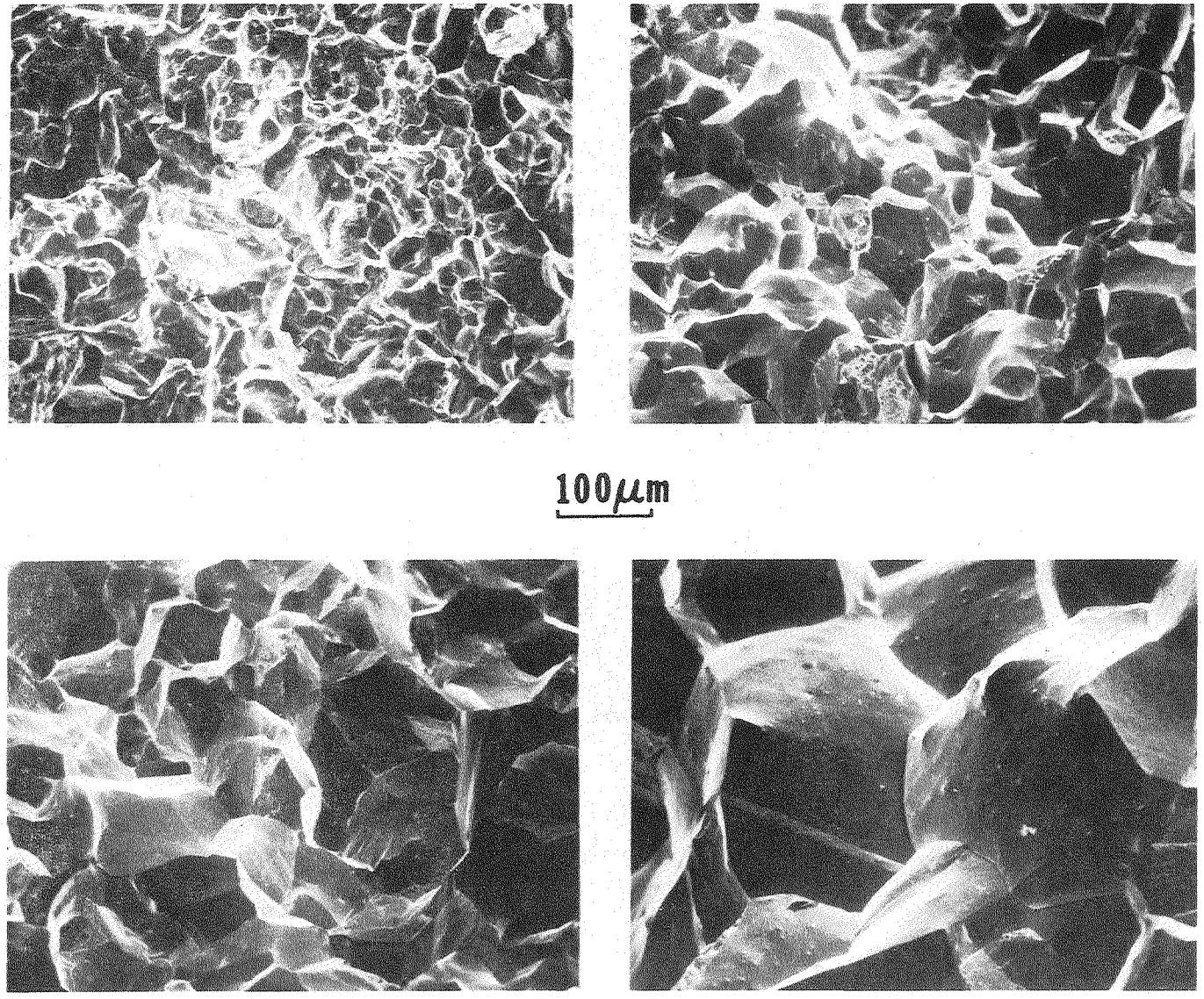

XBB 800-12306

Figure 6

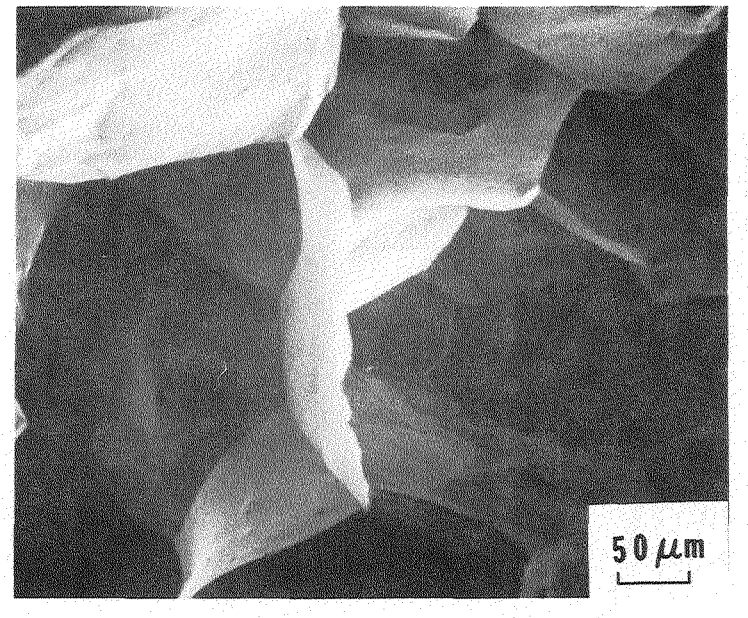

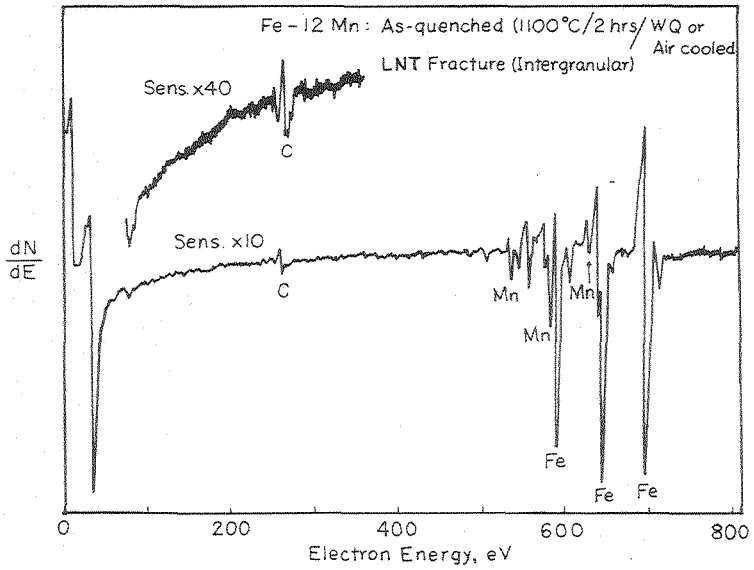

Figure 7

XBB 812-1600

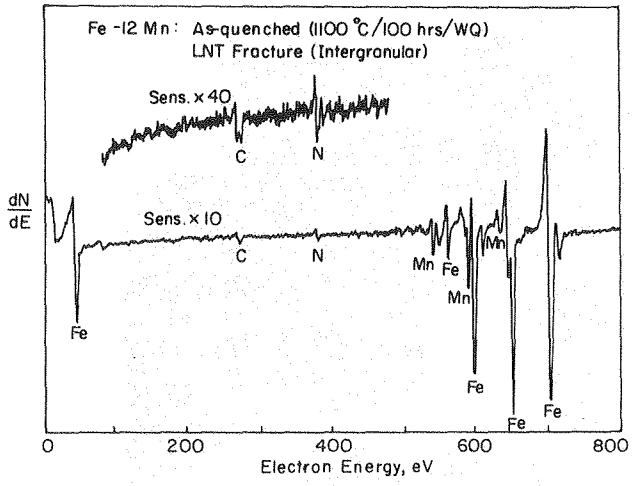

Figure 8 XBL 8011-12713

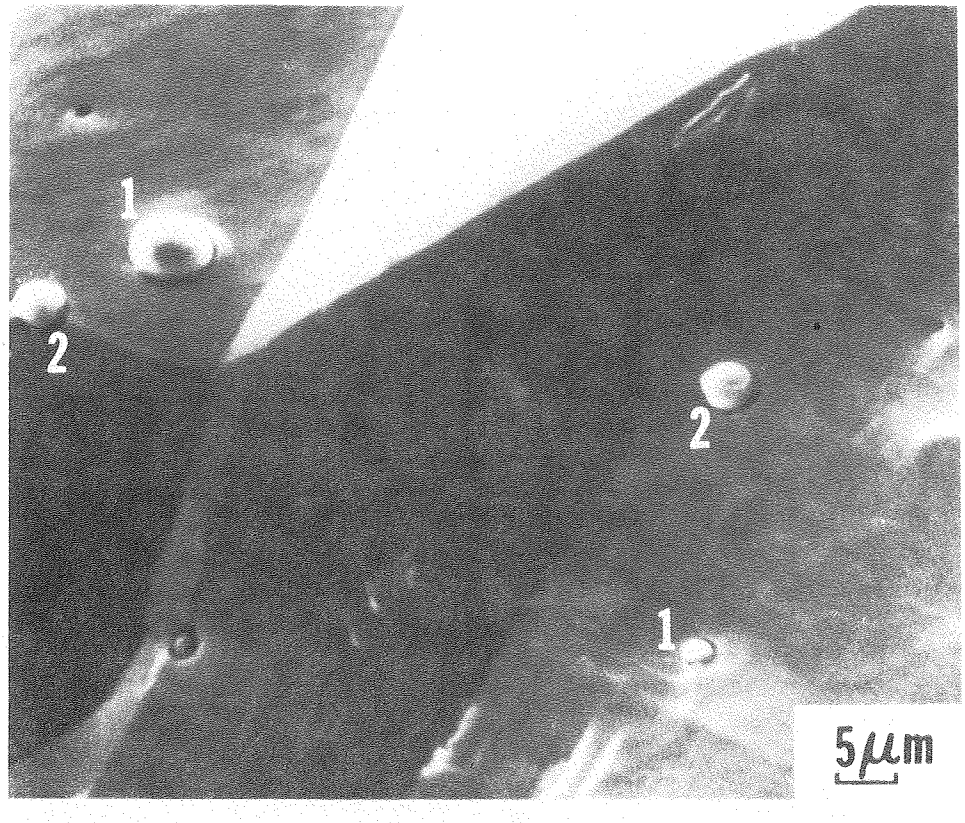

1.

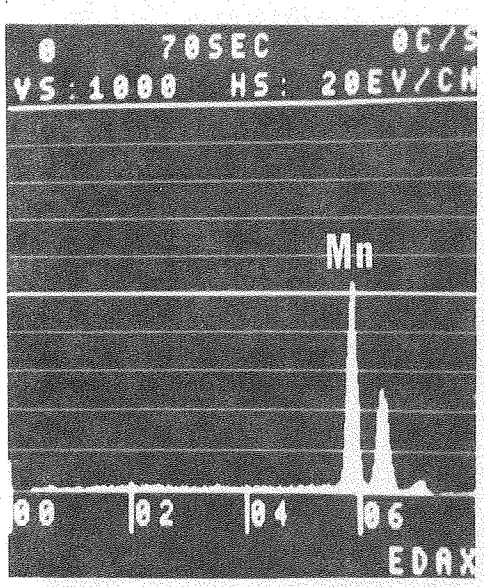

2.

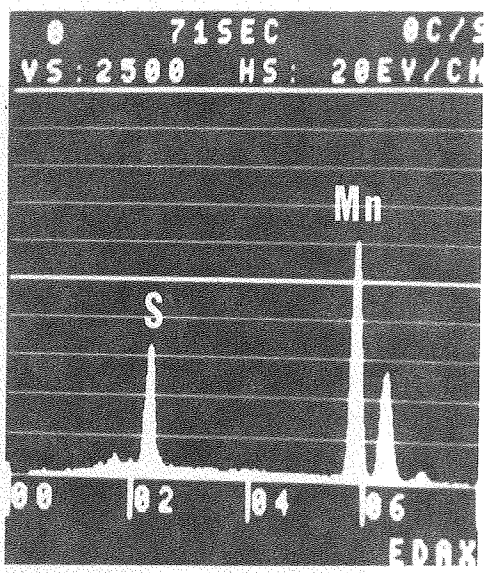

XBB 800-12307

Figure 9

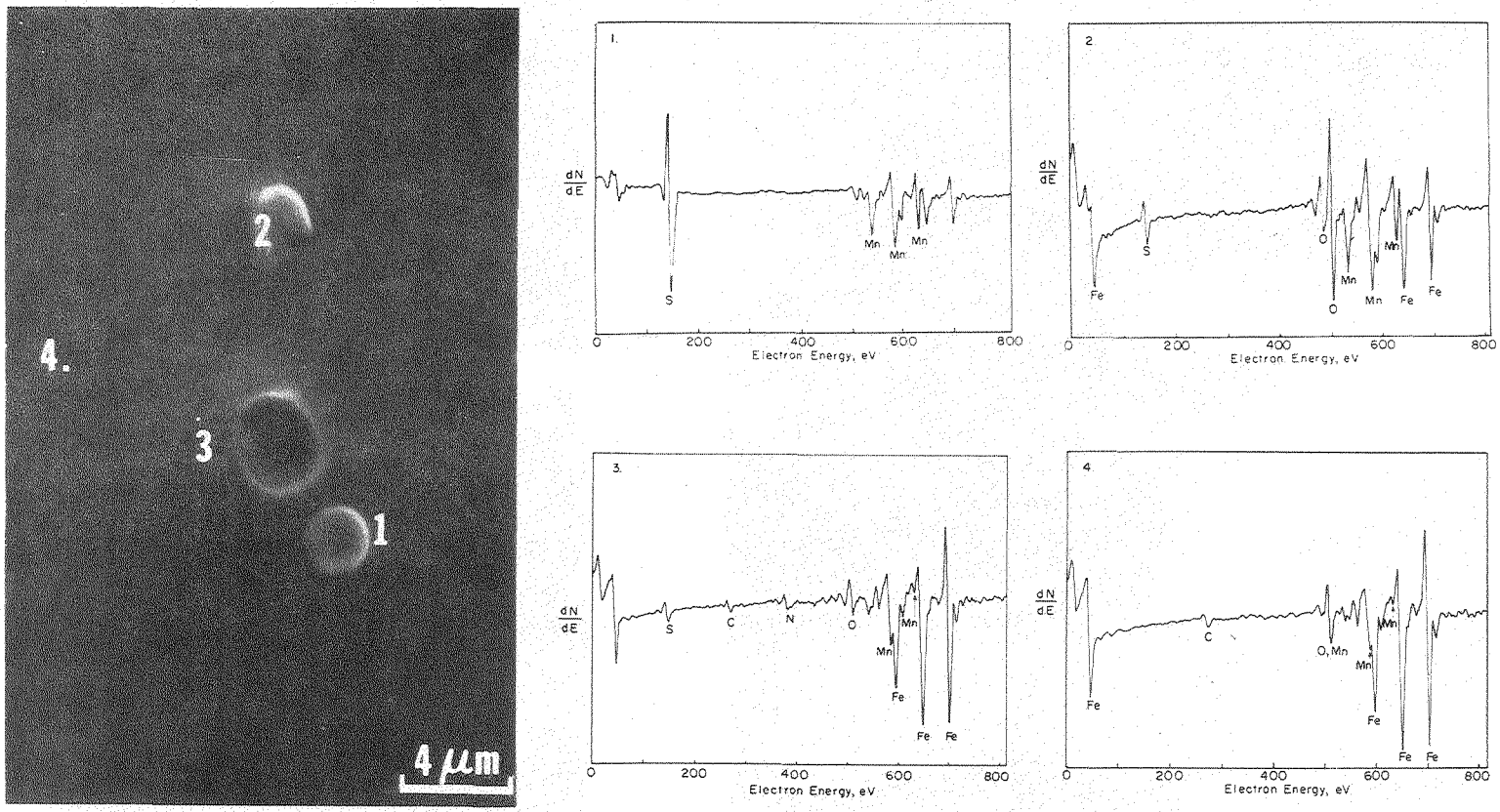

Figure 10

XBB 800-13508

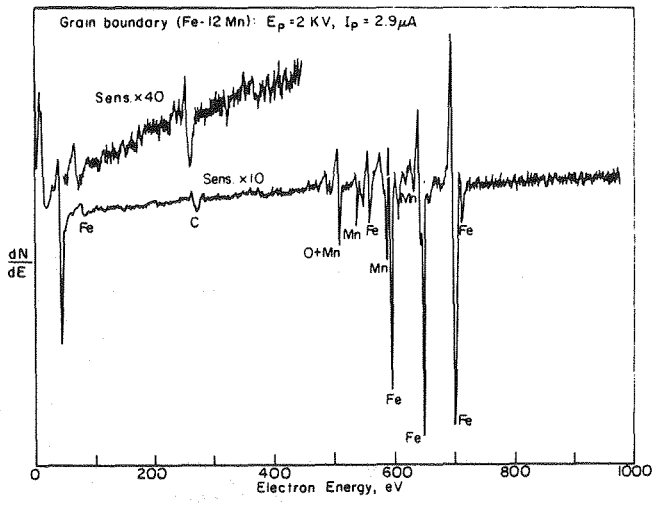

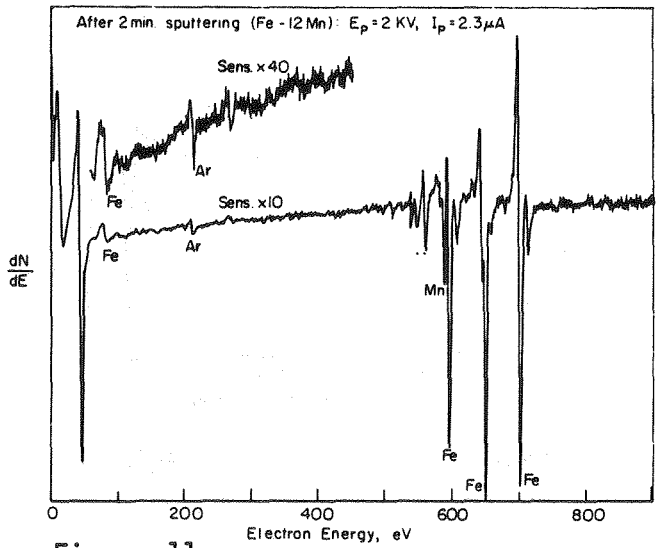

Figure 11

X8L804-5051

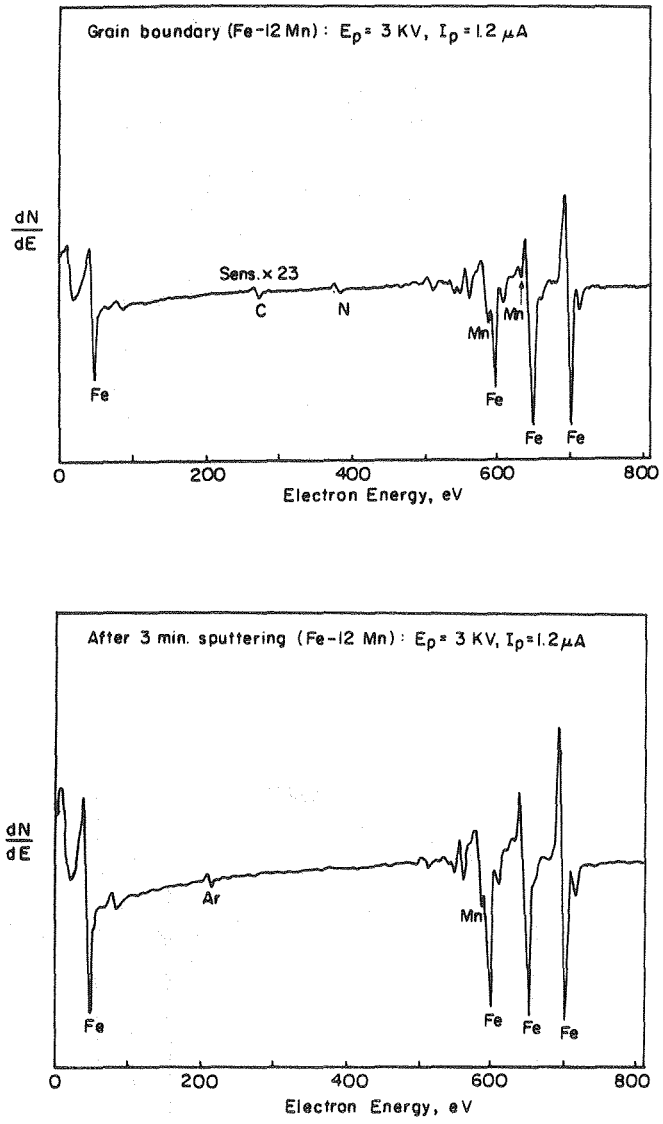

Figure 12 XBL 8011-12714

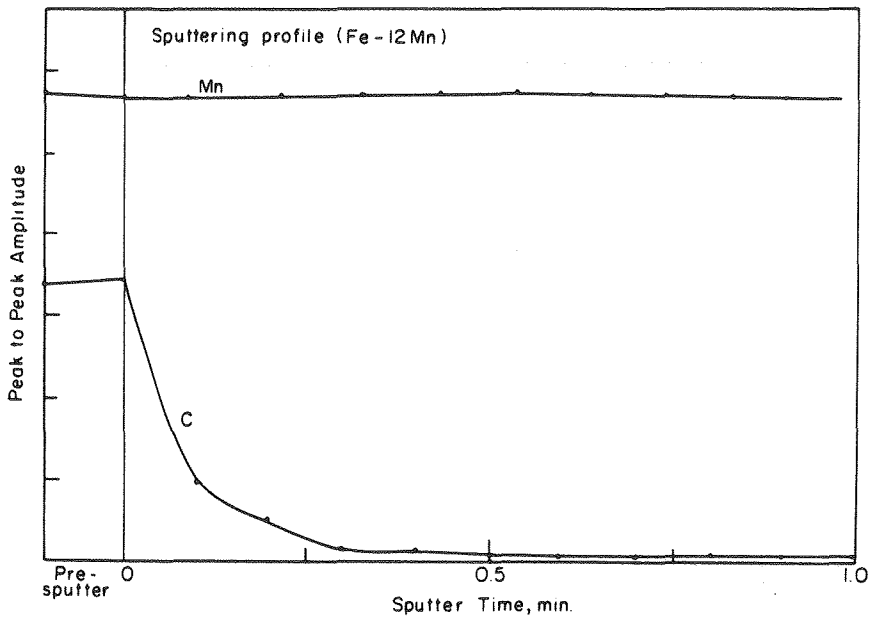

XBL 804-5060

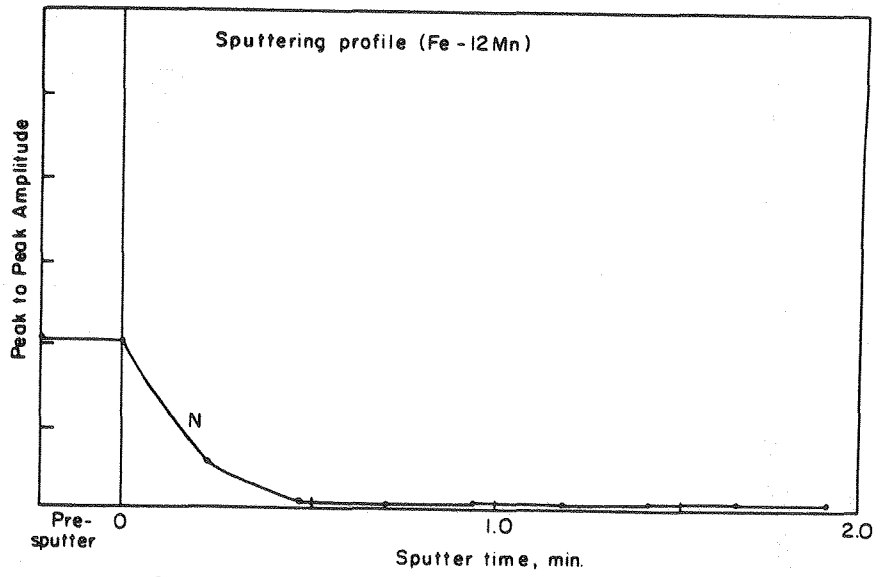

Figure 13

XBL 8010-6243

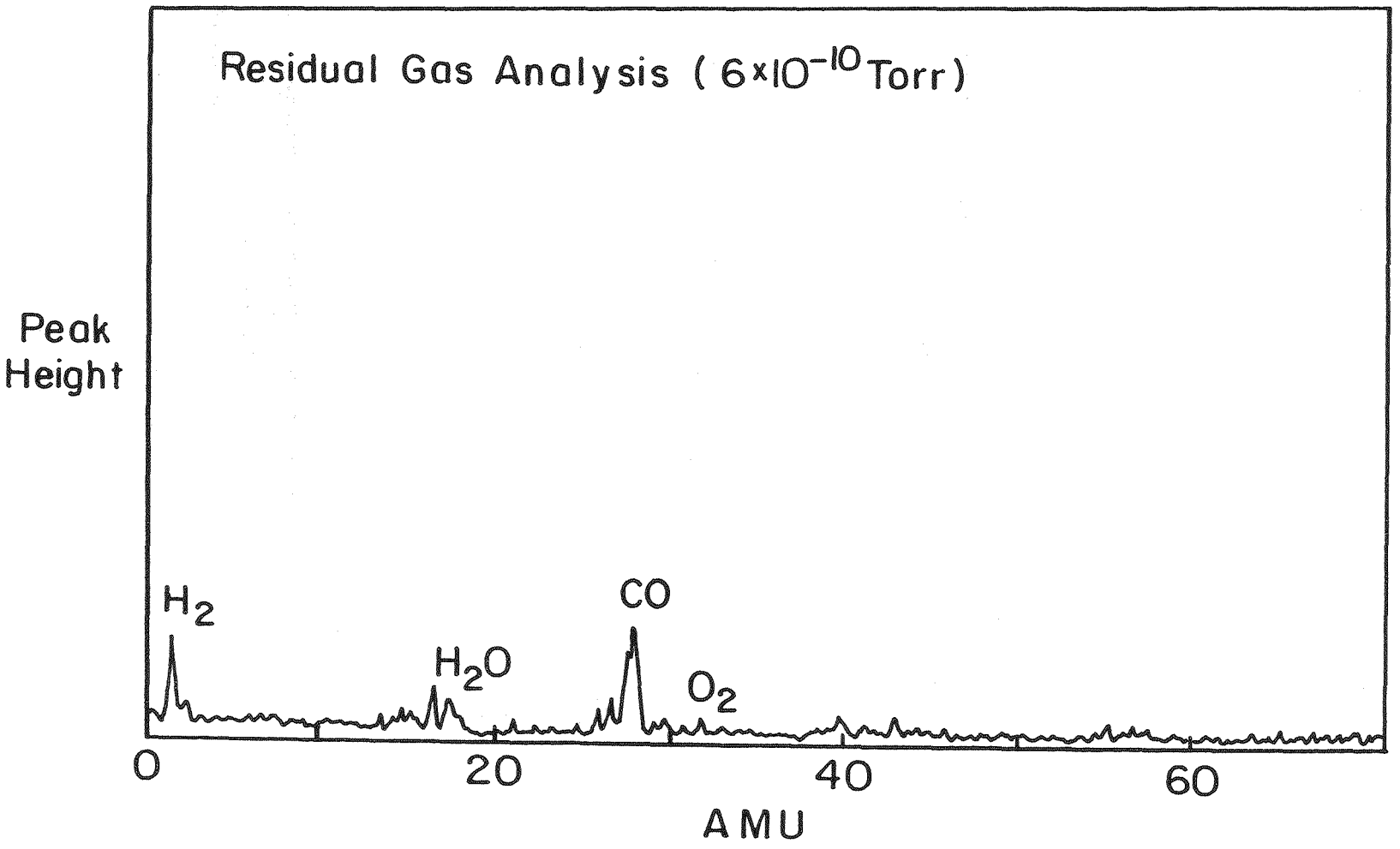

Figure 14

XBL 8010-6242A

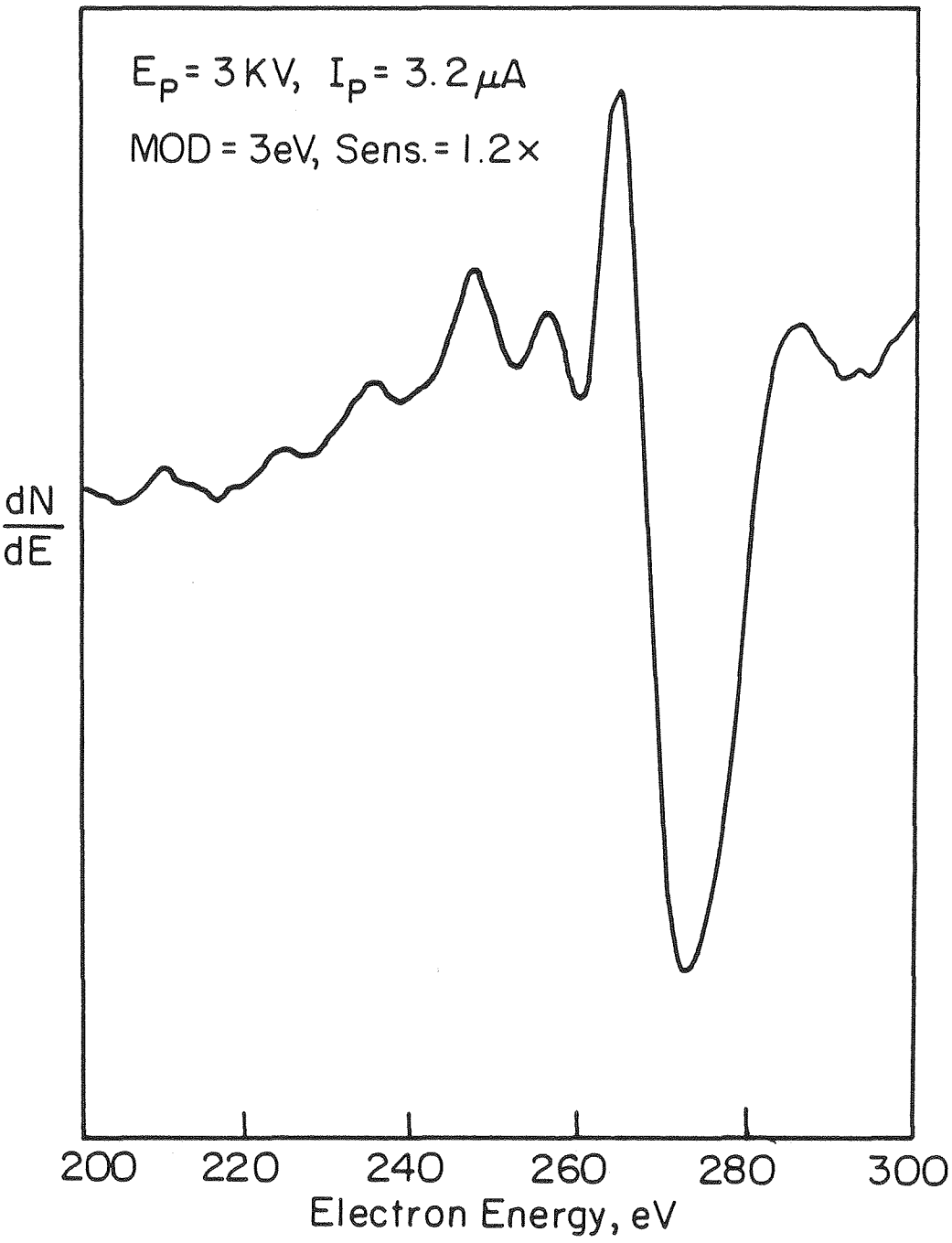

Figure 15

XBL804-5058